

Challenging lanthanide relaxation theory: erbium and thulium complexes that show NMR relaxation rates faster than dysprosium and terbium analogues

Alexander M. Funk, Peter Harvey, Katie-Louise N. A. Finney, Mark A. Fox,
Alan M. Kenwright, Nicola J Rogers, P. Kanthi Senanayake and David Parker.

Department of Chemistry, Durham University, South Road, Durham, DH1 3LE, UK.

Contents

General Experimental

ESI Figure 1 Variation of the longitudinal relaxation rate, R_1 with magnetic field for the ^1Bu resonance in $[\text{Er}.\text{L}^3]$, showing the fit ($T_{1e} = 0.88 \text{ ps}$; $\mu_{\text{eff}} = 9.7 \text{ BM}$) to the data at six fields (295K, D_2O , fixing $r = 6.6 \text{ \AA}$ and $\tau_r = 260 \text{ ps}$).

ESI Figure 2 Simulation of the longitudinal relaxation rate, R_1 with magnetic field for an idealised resonance in a hypothetical lanthanide (III) complex, ($r = 6.6 \text{ \AA}$ and $\tau_r = 260 \text{ ps}$, 295K), for the following values and using literature data for μ_{eff} . Tb: $T_{1e} = 0.57 \text{ ps}$; $\mu_{\text{eff}} = 9.8 \text{ BM}$; Dy, $T_{1e} = 0.45 \text{ ps}$; $\mu_{\text{eff}} = 10.3 \text{ BM}$; Ho: $T_{1e} = 0.39 \text{ ps}$; $\mu_{\text{eff}} = 10.4 \text{ BM}$; Er: $T_{1e} = 0.97 \text{ ps}$; $\mu_{\text{eff}} = 9.4 \text{ BM}$; Tm: $T_{1e} = 0.48 \text{ ps}$; $\mu_{\text{eff}} = 7.6 \text{ BM}$. These T_{1e} values are those used in Figure 1 (main text), and define the low field relaxation behaviour.

ESI Figure 3 Shift and relaxation data for the Er and Dy analogues (295K, D_2O), showing the two major isomeric species.

ESI Figure 4: Simulation of the dependence of the ^1H NMR R_1 and R_2 values in an idealized complex on the rotational correlation time, τ_R , at different field strengths (295 K, $\mu_{\text{eff}} = 10 \text{ BM}$, $T_{1e} = 0.5 \text{ ps}$, $r = 6.5 \text{ \AA}$).

ESI Figure 5 : ^{19}F NMR relaxation (R_1 / s^{-1}) for the CF_3 resonance in $[\text{Ln}.\text{L}^1]$ as a function of field, showing the fit (lines) to experimental data (points) (295 K, D_2O).

ESI Figure 6 : ^1H NMR relaxation (R_1 / s^{-1}) for the ^1Bu resonance in $[\text{Ln}.\text{L}^4]$ as a function of magnetic field, showing the fit (lines) to the data (points) (295 K, D_2O).

ESI Figure 7 : ^1H NMR relaxation (R_1 / s^{-1}) for the pyH^5 resonance in $[\text{Ln}.\text{L}^5]$ as a function of magnetic field, showing the fit (lines) to the data (points) (295 K, D_2O).

ESI Figure 8 : ^1H NMR relaxation (R_1 / s^{-1}) for the pyH^5 resonance in $[\text{Ln}.\text{L}^6]$ as a function of magnetic field, showing fit (lines) to the data (points) (295 K, CD_3OD).

ESI Figure 9 : ^1H NMR relaxation (R_1 / s^{-1}) for the pyH^5 resonance in $[\text{Ln}.\text{L}^7]^{3+}$ as a function of magnetic field, showing fit (lines) to the data (points) (295 K, CD_3OD).

ESI Figure 10 : ^1H NMR chemical shift (δ / ppm) of the ^1Bu resonance of $[\text{Dy}.\text{L}^3]$ at 11.7 T as a function of $1/T^2$ in the temperature range 290-315 K, showing experimental data (points) and linear regression (D_2O).

Tables 1-8: Relaxation rate data for complexes $[\text{Ln}.\text{L}^{5-7}]$ as a function of magnetic field.

General Experimental

Details of the syntheses and characterization data for the complexes described here have been reported recently.^{5,7,8,10,11}

General NMR procedures

¹H, ¹⁹F and ³¹P NMR spectra were obtained at 295 K (unless stated otherwise) on Varian spectrometers operating at 4.7, 9.4, 11.7, 14.1, 16.5 Tesla, specifically on a Mercury 200 spectrometer (¹H at 200.057 MHz, ¹⁹F at 188.242 MHz, ³¹P at 80.985 MHz), a Mercury 400 spectrometer (¹H at 399.97 MHz, ¹⁹F at 376.331 MHz, ³¹P at 161.910 MHz), a Varian Inova-500 spectrometer (¹H at 499.78 MHz, ¹⁹F at 470.322 MHz, ³¹P at 202.340 MHz), a Varian VNMRS-600 spectrometer (¹H at 599.944 MHz, ¹⁹F at 564.511 MHz, ³¹P at 242.862 MHz) and a Varian VNMRS-700 spectrometer (¹H at 700.000 MHz, ¹⁹F at 658.658 MHz, ³¹P at 283.365 MHz). Commercially available deuterated solvents were used. Measurements at 1T (42.5MHz ¹H) were made on a Magritek Spinsolve spectrometer. Samples were inserted at 295K and T_1 measurements were made over the range 295-301K, using the temperature dependence of the t-Bu shift (1/T² dependence) to estimate the measurement temperature.

The operating temperature of the other spectrometers was measured with the aid of an internal calibration sample of neat ethylene glycol for high temperature studies. A calibration sample of freshly distilled methanol was used for low temperatures studies. The operating temperature of each spectrometer was measured before each set of measurements of relaxation data.

The ¹⁹F and ³¹P relaxation data were measured without proton decoupling. The ¹⁹F chemical shifts are reported relative to fluorotrichloromethane.

The recorded free induction decays were processed using backward linear prediction, optimal exponential weighting, zero-filling, Fourier transform, phasing and baseline correction (by Whittaker smoothing), if necessary.

Relaxation data analysis

The nuclear relaxation times of the nuclei of interest were measured at the 5 or 6 different fields mentioned above. The T_1 values were measured using the inversion-recovery technique. At first a crude T_1 value was obtained, which was then used as the initial guess in multiple repeat experiments. The incremented delay time was set to show full inversion and full recovery to equilibrium of the signal, which is roughly achieved at five times the T_1 value.

The concentration of a sample was kept constant throughout a series of measurements, which was in the range of 0.1 to 1 mM. For each complex studied the ¹H, ¹⁹F relaxation data considered in this work can be found in the references given in the main text.

The measured nuclear relaxation data was fitted by using a modified Matlab algorithm originally written by Dr. Ilya Kuprov of Southampton University. The algorithm uses the Solomon-Morgan-Bloembergen equation (1) to fit the measured relaxation data using the Matlab internal Levenberg-Marquardt minimisation of the non-linear squares error function. The results were analysed iteratively

and it was assumed that the longitudinal and transverse electronic relaxation times were of a similar magnitude.

$$R_1 = \frac{2}{15} \left(\frac{\mu_0}{4\pi} \right)^2 \frac{\gamma_N^2 g_{\text{Ln}}^2 \mu_B^2 J(J+1)}{r^6} \left[3 \frac{T_{1e}}{1 + \omega_N^2 T_{1e}^2} + 7 \frac{T_{1e}}{1 + \omega_e^2 T_{1e}^2} \right] \\ + \frac{2}{5} \left(\frac{\mu_0}{4\pi} \right)^2 \frac{\omega_N^2 \mu_{\text{eff}}^4}{(3k_B T)^2 r^6} \left[3 \frac{\tau_r}{1 + \omega_N^2 \tau_r^2} \right]$$

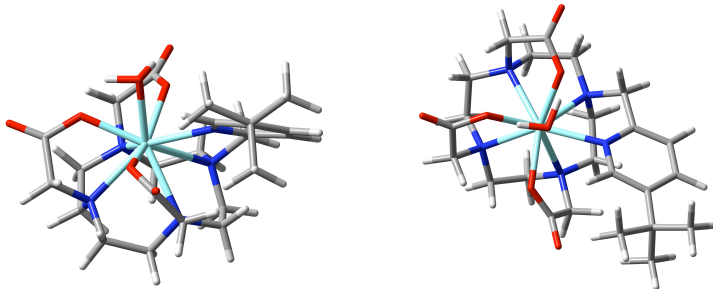
Some parameters were used globally for every lanthanide(III) complex in the series and others were used for each complex individually. The rotational correlation time, τ_r , was considered not to vary across a given series of complexes in a given solvent at 295K. An estimate for τ_r was determined by the Stokes-Einstein Law in which estimates of the hydrodynamic radius, r , were made by inspecting the X-ray data; in each case a reasonable agreement was found (± 0.2 Å).

Error Analysis

Each relaxation measurement was repeated at least three times on different samples, and the mean value recorded. The number of transients used in the measurements was determined by the signal-to-noise ratio and also by the linewidth of the resonance of interest. In each case, the signal was fully recovered during the inversion-recovery sequence.

A statistical error analysis was undertaken to determine the fitting errors. The experimental errors of the measured relaxation rates were combined and used to perturb the relaxation rates for each complex at each field. These perturbed rates together with the unperturbed relaxation rates were used in a statistical error analysis to obtain the error values for the individual parameters (μ_{eff} , r , τ_r and T_{1e}) calculated in the fitting process.

Ab initio and DFT Computations



The model geometry for [Y.L²(H₂O)] was fully optimised without symmetry constraints using the B3LYP functional and ⁱ 3-21G* basis set ⁱⁱ for all atoms with the Gaussian 09 package.ⁱⁱⁱ A frequency calculation confirmed the geometry to be a true minimum.

The mean Y...H (butyl) distance of 6.62 Å was obtained as the average of all nine Y...H (butyl) distances; the shortest and longest distances measured at 5.315 and 7.916 Å respectively. Geometry optimisations were also carried out with various combinations of Hartree-Fock (HF), BLYP, B3LYP functionals and the STO-3G and 3-21G* basis sets and the Y...H(butyl) distances from these optimised geometries are listed in Table 9. The mean Y...H(butyl) distances of these optimised

geometries are all longer (by up to 0.377 Å for BLYP/STO-3G) than the B3LYP/3-21G* model geometry and the estimated experimental values, derived by global fitting of the rate data. The starting point for the Y complex geometry used was the X-ray crystal structure of a mono-aqua Gd complex of a 4-morpholino-2-methylpyridine derivative of ‘DO3A’ (CCDC: 440/112; S. Aime, A.S. Batsanov, M. Botta, J.A.K. Howard, M.P. Lowe and D. Parker, *New. J. Chem.* 1999, **23**, 669).

ESI Table Mean, shortest and longest Y...H(butyl) distances in the six optimised geometries of [Y.L²(H₂O)].

Functional/Basis Set	mean	shortest	longest
B3LYP/3-21G*	6.622	5.135	7.916
B3LYP/STO-3G	6.904	5.528	7.942
BLYP/3-21G*	6.677	5.174	7.986
BLYP/STO-3G	6.999	5.625	8.046
HF/3-21G*	6.694	5.223	7.768
HF/STO-3G	6.812	5.427	7.821

Cartesian coordinates for [Y.L²(H₂O)]

```

Y      0.730162 -0.110957 -0.365159
O     -0.522407 -1.981457 -0.264880
O     -2.561953 -2.887331  0.265206
O      2.006399 -1.150339 -1.895322
O      3.618541 -2.689413 -2.419559
O      1.087043  1.775578 -1.612326
O      2.465545  3.486322 -2.254238
O     -0.239332 -0.158961 -2.600422
N      0.697028  2.003797  1.265193
N     -0.251353 -0.671769  2.099578
N      2.189918 -1.895322  0.760089
N      3.124815  0.796621 -0.013056
N     -1.504186  0.961128 -0.288422
C      0.483539  1.646213  2.709188
C     -0.576382  0.560891  2.897000
C      0.806705 -1.471049  2.811249
C      1.449603 -2.525989  1.908440
C      3.512845 -1.351666  1.223783
C      4.094972 -0.330291  0.239632
C      3.199321  1.790174  1.112844
C      2.005411  2.752187  1.140603
C     -0.424226  2.874709  0.741710
C     -1.489974 -1.502386  1.897565
C     -1.543548 -2.212153  0.519885
C      2.389702 -2.915772 -0.335843
C      2.745256 -2.233556 -1.674036
C      3.440407  1.460879 -1.331632
C      2.269869  2.355994 -1.789913
C     -1.681497  2.098387  0.418049
C     -2.964595  2.545424  0.729424
C     -4.067051  1.787821  0.324384
C     -3.893939  0.619115 -0.434573
C     -2.574915  0.270558 -0.742794
H      0.518171 -0.742905 -2.912721
H      0.080923  0.790515 -2.722764
H      0.194284  2.540319  3.285306

```

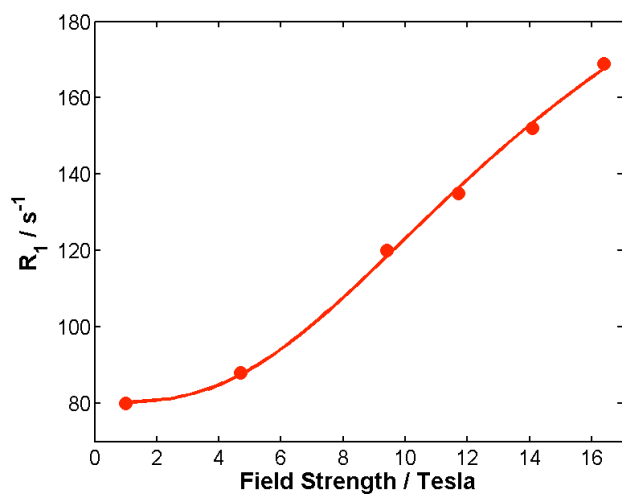
H	1.441291	1.298796	3.104801
H	-0.670929	0.327903	3.969710
H	-1.538605	0.933257	2.546846
H	0.367686	-1.970154	3.690609
H	1.569554	-0.776962	3.172364
H	2.122629	-3.158096	2.507371
H	0.673542	-3.152799	1.474320
H	4.233257	-2.172655	1.362418
H	3.359233	-0.877380	2.197000
H	5.042522	0.058805	0.643062
H	4.313878	-0.811673	-0.712444
H	4.127013	2.379427	1.036771
H	3.241287	1.228387	2.050395
H	2.129862	3.443603	1.988968
H	1.985558	3.349621	0.230929
H	-0.057889	3.274377	-0.208562
H	-0.641158	3.695258	1.440390
H	-2.360151	-0.841814	1.932269
H	-1.610600	-2.245985	2.697522
H	1.421280	-3.403650	-0.478536
H	3.160571	-3.647042	-0.068044
H	3.531401	0.653026	-2.062551
H	4.363717	2.048413	-1.276601
H	-3.099065	3.464346	1.287533
H	-2.333495	-0.579426	-1.359864
H	-5.062553	2.113810	0.599543
C	-5.064565	-0.300976	-0.811128
C	-4.657237	-1.311692	-1.913883
H	-4.284249	-0.796919	-2.806841
H	-3.897023	-2.004474	-1.538184
H	-5.539016	-1.897643	-2.196522
C	-5.435219	-1.115882	0.463385
H	-4.590431	-1.758412	0.735957
H	-5.688811	-0.449558	1.296687
H	-6.302447	-1.752322	0.250114
C	-6.280557	0.524570	-1.297185
H	-7.093877	-0.158384	-1.565457
H	-6.654215	1.199111	-0.518568
H	-6.017240	1.117138	-2.180309

¹. (i) A. D. Becke, *J. Chem. Phys.*, 1993, **98**, 5648-5652; (b) C. Lee, W. Yang and R. G. Parr, *Phys. Rev. B*, 1988, **37**, 785-789.

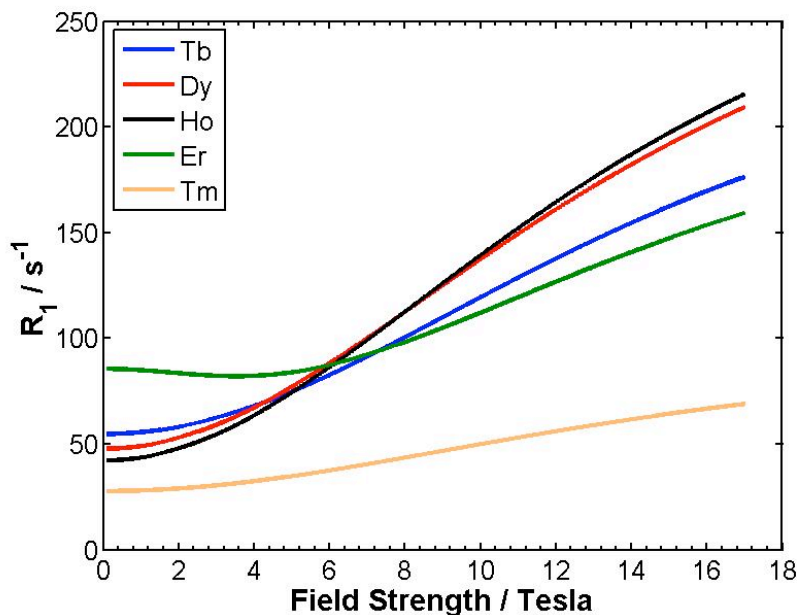
¹. (ii) J. S. Binkley, J. A. Pople and W. J. Hehre, *J. Am. Chem. Soc.*, 1980, **102**, 939-947; (b) M. S. Gordon, J. S. Binkley, J. A. Pople, W. J. Pietro and W. J. Hehre, *J. Am. Chem. Soc.*, 1982, **104**, 2797-2803; (c) W. J. Pietro, M. M. Franci, W. J. Hehre, D. J. Defrees, J. A. Pople and J. S. Binkley, *J. Am. Chem. Soc.*, 1982, **104**, 5039-5048; (d) K. D. Dobbs and W. J. Hehre, *J. Comp. Chem.*, 1986, **7**, 359-378; (e) K. D. Dobbs and W. J. Hehre, *J. Comp. Chem.*, 1987, **8**, 861-879; (f) K. D. Dobbs and W. J. Hehre, *J. Comp. Chem.*, 1987, **8**, 880-893.

¹ (iii) Gaussian 09, Revision A.02, M. J. Frisch, G. W. Trucks, H. B. Schlegel, G. E. Scuseria, M. A. Robb, J. R. Cheeseman, G. Scalmani, V. Barone, B. Mennucci, G. A. Petersson, H. Nakatsuji, M. Caricato, X. Li, H. P. Hratchian, A. F. Izmaylov, J. Bloino, G. Zheng, J. L. Sonnenberg, M. Hada, M. Ehara, K. Toyota, R. Fukuda, J. Hasegawa, M. Ishida, T. Nakajima, Y. Honda, O. Kitao, H. Nakai, T. Vreven, Jr., J. A. Montgomery, J. E. Peralta, F. Ogliaro, M. Bearpark, J. J. Heyd, E. Brothers, K. N. Kudin, V. N. Staroverov, R. Kobayashi, J. Normand, K. Raghavachari, A. Rendell, J. C. Burant, S. S. Iyengar, J.

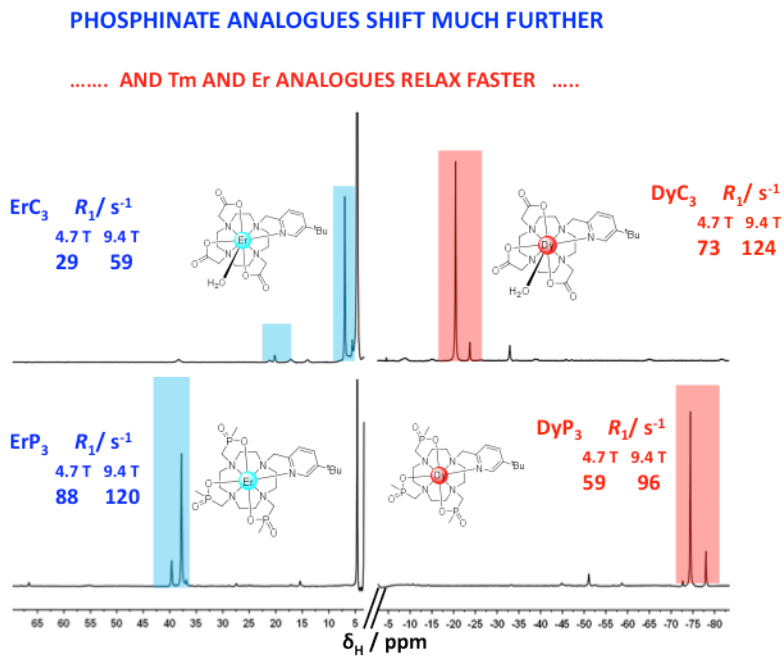
Tomasi, M. Cossi, N. Rega, J. M. Millam, M. Klene, J. E. Knox, J. B. Cross, V. Bakken, C. Adamo, J. Jaramillo, R. Gomperts, R. E. Stratmann, O. Yazyev, A. J. Austin, R. Cammi, C. Pomelli, J. W. Ochterski, R. L. Martin, K. Morokuma, V. G. Zakrzewski, G. A. Voth, P. Salvador, J. J. Dannenberg, S. Dapprich, A. D. Daniels, O. Farkas, J. B. Foresman, J. V. Ortiz, J. Cioslowski and D. J. Fox, *Gaussian, Inc.*, Wallingford CT, **2009**.

Figures

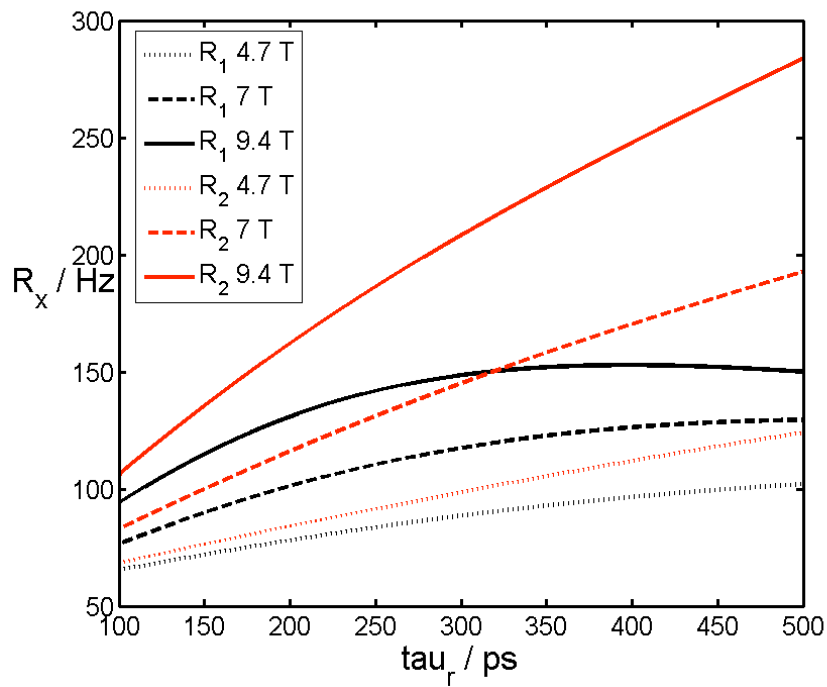
ESI Figure 1 Variation of the longitudinal relaxation rate, R_1 with magnetic field for the ${}^1\text{Bu}$ resonance in $[\text{Er.L}^3]$, showing the fit ($T_{1\text{e}} = 0.85$ ps; $\mu_{\text{eff}} = 9.7$ BM) to the data at six fields (295K, D₂O, fixing $r = 6.6$ Å and $\tau_r = 260$ ps).



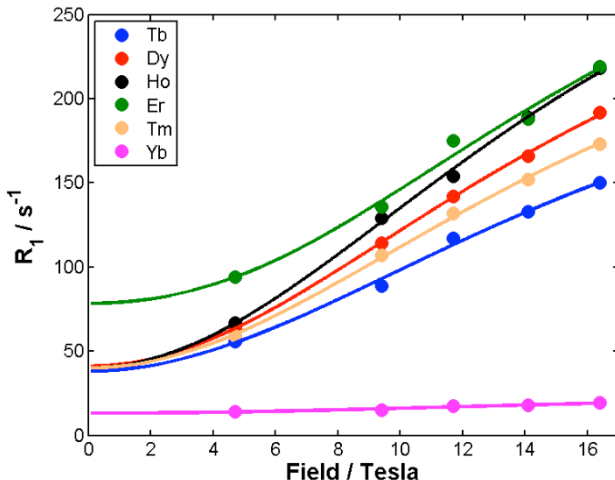
ESI Figure 2 Simulation of the longitudinal relaxation rate, R_1 with magnetic field for an idealised resonance in a hypothetical lanthanide (III) complex, ($r = 6.6$ Å and $\tau_r = 260$ ps, 295K), for the following values and using literature data for μ_{eff} . Tb: $T_{1\text{e}} = 0.57$ ps; $\mu_{\text{eff}} = 9.8$ BM; Dy, $T_{1\text{e}} = 0.45$ ps; $\mu_{\text{eff}} = 10.3$ BM; Ho: $T_{1\text{e}} = 0.39$ ps; $\mu_{\text{eff}} = 10.4$ BM; Er: $T_{1\text{e}} = 0.97$ ps; $\mu_{\text{eff}} = 9.4$ BM; Tm: $T_{1\text{e}} = 0.48$ ps; $\mu_{\text{eff}} = 7.6$ BM. These $T_{1\text{e}}$ values define the low field relaxation behaviour.



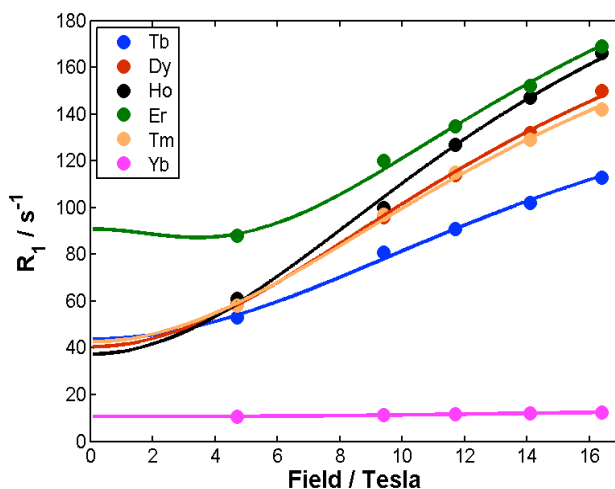
ESI Figure 3 Shift and relaxation data for the Er and Dy analogues (295K, D₂O), showing the two major isomeric species.



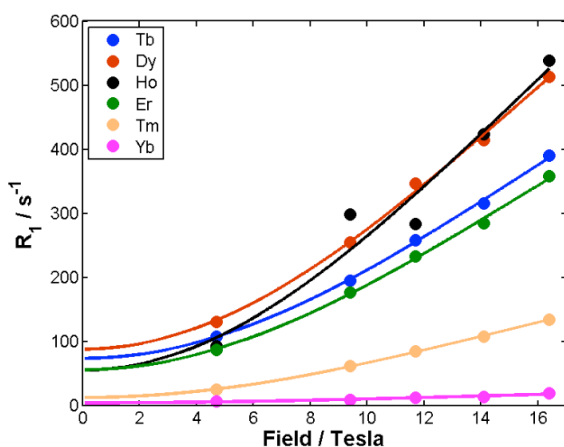
ESI Figure 4 Simulation of the dependence of the ¹H NMR R_1 and R_2 values in an idealized complex on the rotational correlation time, τ_R , at different field strengths (295 K, $\mu_{\text{eff}} = 10$ BM, $T_{le} = 0.5$ ps, $r = 6.5$ Å).



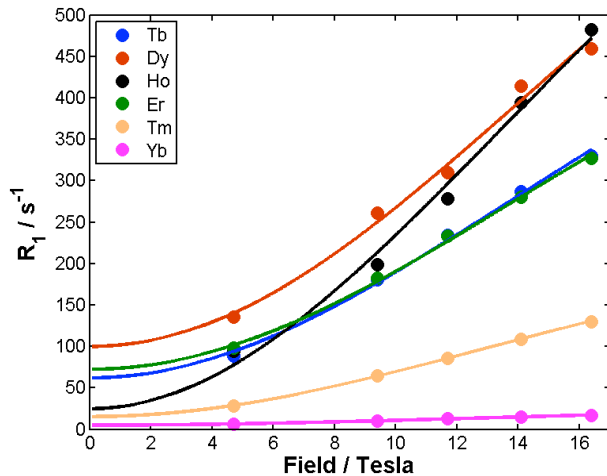
ESI Figure 5 ^{19}F NMR relaxation rates($\text{R}_1 / \text{s}^{-1}$) for CF_3 resonance in $[\text{Ln}.\text{L}^1]$ as a function of magnetic field, showing the fit (lines) to the experimental data (points) (295 K, D_2O).



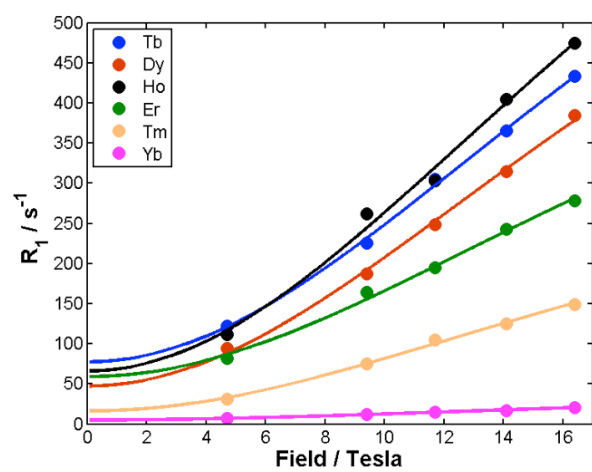
ESI Figure 6 ^1H NMR relaxation ($\text{R}_1 / \text{s}^{-1}$) for the ^1Bu resonance in $[\text{Ln}.\text{L}^4]$ as a function of magnetic field, showing the fit (lines) to the experimental data (points) (295 K, D_2O).



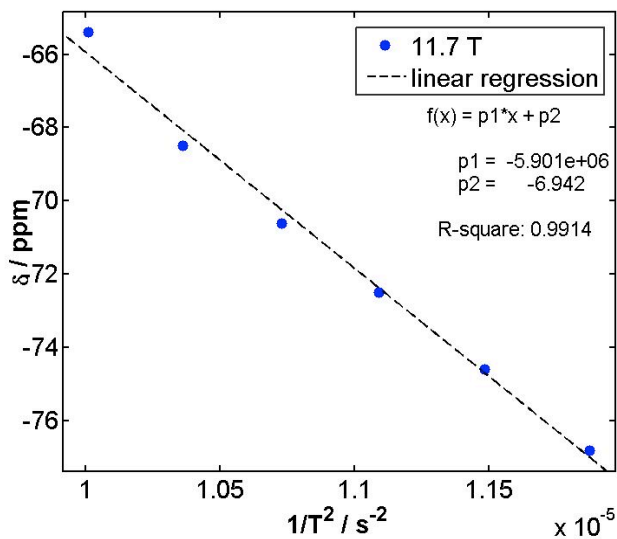
ESI Figure 7 ^1H NMR relaxation ($\text{R}_1 / \text{s}^{-1}$) for the pyH^3 resonance in $[\text{Ln}.\text{L}^5]$ as a function of magnetic field, showing the fit (lines) to the experimental data (points) (295 K, D_2O).



ESI Figure 8 ^1H NMR relaxation (R_1 / s^{-1}) for the pyH 5 resonance in $[\text{Ln.L}^6]$ as a function of magnetic field, showing the fit (lines) to the experimental data (points) (295 K, CD₃OD).

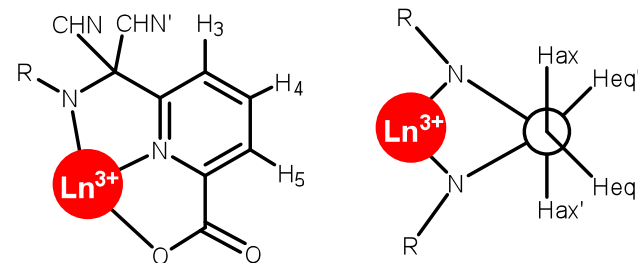


ESI Figure 9 ^1H NMR relaxation (R_1 / s^{-1}) for the pyH 5 resonance in $[\text{Ln.L}^7]^{3+}$ as a function of magnetic field, showing the fit (lines) to the experimental data (points) (295 K, CD₃OD).



ESI Figure 10 ^1H NMR chemical shift (δ / ppm) of the ^tBu resonance of $[\text{Dy}.\text{L}^3]$ at 11.7 T as a function of $1/\text{T}^2$ in the temperature range 290-315 K, showing experimental data (points) and linear regression (D_2O).

ESI-Table 1 ^1H nuclear relaxation rates, R_1 , of the pyH^3 resonance in $[\text{Ln}.\text{L}^5]$ (295 K, D_2O).



^1H	R_1 / s^{-1}				
	4.7 T	9.4 T	11.7 T	14.1 T	16.5 T
Tb	108 ± 6	195 ± 5	258 ± 5	316 ± 9	390 ± 15
Dy	130 ± 7	255 ± 3	347 ± 6	414 ± 20	513 ± 11
Ho	92 ± 11	298 ± 27	283 ± 51	423 ± 51	538 ± 51
Er	87 ± 5	176 ± 8	233 ± 13	284 ± 27	358 ± 48
Tm	25 ± 1	61 ± 0.3	84 ± 0.2	108 ± 0.3	134 ± 0.5
Yb	5.7 ± 0.2	9.5 ± 0.5	12.5 ± 0.1	12.8 ± 0.7	18.6 ± 0.2

ESI-Table 2 ^1H nuclear relaxation rates, R_1 , of the pyH^4 resonance in $[\text{Ln}.\text{L}^5]$ (295 K, D_2O).

^1H	R_1 / s^{-1}				
	4.7 T	9.4 T	11.7 T	14.1 T	16.5 T
Tb	44 ± 3	85 ± 5	131 ± 21	152 ± 7	177 ± 12
Dy	64 ± 2	126 ± 1	164 ± 2	211 ± 3	258 ± 3
Ho	48 ± 2	103 ± 2	142 ± 5	184 ± 3	232 ± 6
Er	39 ± 2	68 ± 3	88 ± 4	119 ± 2	140 ± 3
Tm	12 ± 0.2	27 ± 0.2	37 ± 0.1	48 ± 0.2	60 ± 0.3
Yb	3.1 ± 0.1	4.8 ± 0.2	5.8 ± 0.1	7.4 ± 0.4	8.4 ± 0.1

ESI-Table 3 ^1H nuclear relaxation rates, R_1 , of the H_{ax} resonance in $[\text{Ln}.\text{L}^6]$ (295 K, CD_3OD).

^1H	R_1 / s^{-1}				
	4.7 T	9.4 T	11.7 T	14.1 T	16.5 T
Tb	526 \pm 7	1090 \pm 11	1357 \pm 5	1687 \pm 15	2057 \pm 26
Dy	710 \pm 27	1484 \pm 9	1848 \pm 5	2312 \pm 13	2593 \pm 45
Ho	472 \pm 9	1184 \pm 18	1682 \pm 39	1892 \pm 32	2350 \pm 93
Er	485 \pm 11	917 \pm 11	1184 \pm 34	1427 \pm 39	1662 \pm 64
Tm	133 \pm 2	323 \pm 3	430 \pm 3	542 \pm 1	631 \pm 6
Yb	33 \pm 1	51 \pm 1	64 \pm 1	75 \pm 1	87 \pm 1

ESI-Table 4 ^1H nuclear relaxation rates, R_1 , of H_{eq} resonance in $[\text{Ln}.\text{L}^6]$ (295 K, CD_3OD).

^1H	R_1 / s^{-1}				
	4.7 T	9.4 T	11.7 T	14.1 T	16.5 T
Tb	388 \pm 6	806 \pm 13	1031 \pm 12	1143 \pm 31	1471 \pm 27
Dy	632 \pm 28	1620 \pm 52	1759 \pm 54	1923 \pm 62	2036 \pm 23
Ho	458 \pm 7	1076 \pm 26	1367 \pm 37	1658 \pm 36	2166 \pm 38
Er	381 \pm 9	731 \pm 12	938 \pm 31	1120 \pm 33	1319 \pm 52
Tm	104 \pm 1	244 \pm 2	333 \pm 1	415 \pm 1	475 \pm 12
Yb	23 \pm 2	37 \pm 1	46 \pm 1	55 \pm 1	63 \pm 1

ESI-Table 5 ^1H nuclear relaxation rates, R_1 , of pyH^3 resonance in $[\text{Ln}.\text{L}^6]$ (295 K, CD_3OD).

^1H	R_1 / s^{-1}				
	4.7 T	9.4 T	11.7 T	14.1 T	16.5 T
Tb	97 \pm 2	199 \pm 2	252 \pm 2	305 \pm 3	351 \pm 6
Dy	150 \pm 2	282 \pm 5	344 \pm 7	455 \pm 7	518 \pm 11
Ho	92 \pm 4	218 \pm 13	299 \pm 8	382 \pm 8	433 \pm 16
Er	107 \pm 2	192 \pm 2	245 \pm 3	295 \pm 3	343 \pm 6
Tm	30 \pm 1	69 \pm 0.3	92 \pm 1	116 \pm 1	139 \pm 1
Yb	6.2 \pm 0.1	10.5 \pm 0.5	12.7 \pm 0.1	15.0 \pm 0.1	17.1 \pm 0.1

ESI-Table 6 ^1H nuclear relaxation rates, R_1 , of the pyH^5 resonance in $[\text{Ln}.\text{L}^6]$ (295 K, CD_3OD).

^1H	R_1 / s^{-1}				
	4.7 T	9.4 T	11.7 T	14.1 T	16.5 T
Tb	89 \pm 1	181 \pm 1	234 \pm 1	287 \pm 3	330 \pm 6
Dy	136 \pm 2	261 \pm 5	310 \pm 16	414 \pm 13	459 \pm 12
Ho	94 \pm 4	199 \pm 10	278 \pm 19	394 \pm 25	482 \pm 25
Er	98 \pm 1	182 \pm 2	233 \pm 4	280 \pm 3	327 \pm 6
Tm	28 \pm 1	65 \pm 0.4	86 \pm 1	109 \pm 1	130 \pm 0.4
Yb	6.2 \pm 0.1	10.5 \pm 0.5	12.7 \pm 0.1	15.0 \pm 0.1	17.1 \pm 0.1

ESI-Table 7 ^1H nuclear relaxation rates, R_1 , of pyH³ resonance [Ln.L⁷]³⁺ (295 K, CD₃OD).

^1H	R_1 / s^{-1}				
	4.7 T	9.4 T	11.7 T	14.1 T	16.5 T
Tb	122 ± 3	226 ± 4	305 ± 7	365 ± 8	433 ± 10
Dy	94 ± 3	187 ± 5	249 ± 15	315 ± 10	385 ± 22
Ho	112 ± 4	262 ± 10	378 ± 6	405 ± 9	475 ± 45
Er	82 ± 4	164 ± 5	195 ± 5	243 ± 3	278 ± 4
Tm	31 ± 0.3	75 ± 2	105 ± 1	125 ± 2	149 ± 2
Yb	7.4 ± 1	12.0 ± 1	15.3 ± 1	17.4 ± 1	20.6 ± 1

ESI-Table 8 ^1H nuclear relaxation rates, R_1 , of pyH⁴ resonance in [Ln.L⁷]³⁺ (295 K, CD₃OD).

^1H	R_1 / s^{-1}				
	4.7 T	9.4 T	11.7 T	14.1 T	16.5 T
Tb	46 ± 3	93 ± 1	122 ± 1	148 ± 2	168 ± 3
Dy	59 ± 3	114 ± 5	141 ± 6	176 ± 5	212 ± 5
Ho	49 ± 1	116 ± 2	154 ± 1	190 ± 4	217 ± 9
Er	36 ± 2	61 ± 3	93 ± 7	108 ± 7	122 ± 7
Tm	18 ± 0.4	40 ± 2	53 ± 1	63 ± 1	73 ± 1
Yb	5.0 ± 1	7.3 ± 1	8.6 ± 1	10.1 ± 1	10.7 ± 1

ESI- Table 9

(upper): ^1H NMR shift and nuclear relaxation rates of the 'Bu resonance in [Ln.L²(H₂O)] used (295 K, D₂O, τ_f 260 ps, r 6.6 Å) to give the best-fit values of T_{1e}/μ_{eff} ; (centre): shift data and relaxation rates of the 'Bu resonance of [Ln.L³] (295 K, D₂O, τ_f 260 (4) ps, r 6.6 Å); (lower) data for the 'Bu resonance of [Ln.L⁴(H₂O)]⁺ used in fitting (295 K, D₂O, τ_f 280 ps, r 6.6 Å)

[Ln.L ²]	$\delta_{\text{H}}/\text{ppm}$	R_1/s^{-1}						$\mu_{\text{eff}}/\text{BM}$	T_{1e}/ps
		1 T	4.7 T	9.4 T	11.7 T	14.1 T	16.5 T		
Tb	-11.6	56 ± 1	72 ± 1	104 ± 2	128 ± 1	146 ± 1	169 ± 1	9.68 ± 0.02	0.59 ± 0.02
Dy	-20.5	55 ± 2	73 ± 1	124 ± 1	149 ± 1	170 ± 1	210 ± 2	10.22 ± 0.02	0.49 ± 0.02
Ho	-7.4	28 ± 1	45 ± 1	89 ± 1	118 ± 1	144 ± 1	169 ± 1	9.82 ± 0.01	0.22 ± 0.02
Er	+7.0	21 ± 1	29 ± 1	59 ± 1	80 ± 1	97 ± 1	120 ± 1	8.95 ± 0.01	0.17 ± 0.01
Tm	+10.8	18 ± 2	31 ± 1	54 ± 1	64 ± 1	71 ± 1	82 ± 1	8.12 ± 0.03	0.29 ± 0.02
Yb	+6.3	6.1 ± 0.5	6.4 ± 0.1	7.6 ± 0.3	8.6 ± 0.1	9.5 ± 0.1	10.7 ± 0.1	4.44 ± 0.08	0.29 ± 0.03

[Ln.L ³]	$\delta_{\text{H}}/\text{ppm}$	R_1/s^{-1}						$\mu_{\text{eff}}/\text{BM}$	T_{1e}/ps
		1 T	4.7 T	9.4 T	11.7 T	14.1 T	16.5 T		
Tb	-75.9	35 ± 2	53 ± 2	81 ± 2	91 ± 1	102 ± 1	113 ± 1	8.81 ± 0.03	0.49 ± 0.02
Dy	-75.0	40 ± 2	59 ± 1	96 ± 1	114 ± 1	132 ± 1	150 ± 1	9.47 ± 0.02	0.45 ± 0.02
Ho	-31.8	35 ± 1	61 ± 2	100 ± 1	127 ± 1	147 ± 1	166 ± 1	9.77 ± 0.02	0.37 ± 0.02
Er ^a	+38.2	77 ± 2	88 ± 2	120 ± 2	135 ± 1	152 ± 1	169 ± 1	9.70 ± 0.02	0.85 ± 0.01
Tm	+67.0	18 ± 2	55 ± 1	97 ± 1	115 ± 1	129 ± 1	142 ± 1	9.50 ± 0.02	0.31 ± 0.01
Yb	+16.3	11.1 ± 0.1	10.7 ± 0.1	11.4 ± 0.7	11.6 ± 0.6	12.0 ± 0.1	12.4 ± 0.3	4.57 ± 0.09	0.53 ± 0.02

[Ln.L ⁴]	$\delta_{\text{H}}/\text{ppm}$	R_1/s^{-1}						$\mu_{\text{eff}}/\text{BM}$	T_{1e}/ps
		4.7 T	9.4 T	11.7 T	14.1 T	16.5 T			
Tb	-7.2	103 ± 1	151 ± 1	169 ± 1	188 ± 1	207 ± 2	10.26(03)	0.96(04)	
Dy	-17.8	119 ± 1	174 ± 1	203 ± 1	230 ± 1	256 ± 1	10.84(03)	0.93(04)	
Ho	-7.0	56 ± 1	102 ± 2	138 ± 2	156 ± 1	177 ± 4	10.03(03)	0.25(02)	
Er	+3.4	19 ± 1	41 ± 5	53 ± 7	71 ± 9	81 ± 12	n.d.	n.d.	
Tm	+6.2	21 ± 1	40 ± 1	51 ± 1	59 ± 1	68 ± 1	7.84(04)	0.16(05)	
Yb	+9.1	4.7 ± 0.2	7.1 ± 0.1	8.3 ± 0.2	9.6 ± 0.3	10.5 ± 0.2	4.70(10)	0.15(04)	

-
- ⁱ. (a) A. D. Becke, *J. Chem. Phys.*, 1993, **98**, 5648-5652; (b) C. Lee, W. Yang and R. G. Parr, *Phys. Rev. B*, 1988, **37**, 785-789.
- ⁱⁱ. (a) J. S. Binkley, J. A. Pople and W. J. Hehre, *J. Am. Chem. Soc.*, 1980, **102**, 939-947; (b) M. S. Gordon, J. S. Binkley, J. A. Pople, W. J. Pietro and W. J. Hehre, *J. Am. Chem. Soc.*, 1982, **104**, 2797-2803; (c) W. J. Pietro, M. M. Franci, W. J. Hehre, D. J. Defrees, J. A. Pople and J. S. Binkley, *J. Am. Chem. Soc.*, 1982, **104**, 5039-5048; (d) K. D. Dobbs and W. J. Hehre, *J. Comp. Chem.*, 1986, **7**, 359-378; (e) K. D. Dobbs and W. J. Hehre, *J. Comp. Chem.*, 1987, **8**, 861-879; (f) K. D. Dobbs and W. J. Hehre, *J. Comp. Chem.*, 1987, **8**, 880-893.
- ⁱⁱⁱ. Gaussian 09, Revision A.02, M. J. Frisch, G. W. Trucks, H. B. Schlegel, G. E. Scuseria, M. A. Robb, J. R. Cheeseman, G. Scalmani, V. Barone, B. Mennucci, G. A. Petersson, H. Nakatsuji, M. Caricato, X. Li, H. P. Hratchian, A. F. Izmaylov, J. Bloino, G. Zheng, J. L. Sonnenberg, M. Hada, M. Ehara, K. Toyota, R. Fukuda, J. Hasegawa, M. Ishida, T. Nakajima, Y. Honda, O. Kitao, H. Nakai, T. Vreven, Jr., J. A. Montgomery, J. E. Peralta, F. Ogliaro, M. Bearpark, J. J. Heyd, E. Brothers, K. N. Kudin, V. N. Staroverov, R. Kobayashi, J. Normand, K. Raghavachari, A. Rendell, J. C. Burant, S. S. Iyengar, J. Tomasi, M. Cossi, N. Rega, J. M. Millam, M. Klene, J. E. Knox, J. B. Cross, V. Bakken, C. Adamo, J. Jaramillo, R. Gomperts, R. E. Stratmann, O. Yazyev, A. J. Austin, R. Cammi, C. Pomelli, J. W. Ochterski, R. L. Martin, K. Morokuma, V. G. Zakrzewski, G. A. Voth, P. Salvador, J. J. Dannenberg, S. Dapprich, A. D. Daniels, O. Farkas, J. B. Foresman, J. V. Ortiz, J. Cioslowski and D. J. Fox, *Gaussian, Inc.*, Wallingford CT, **2009**.